

Optical Engineering

SPIEDigitalLibrary.org/oe

Ultrahigh bit-rate all-optical multibit correlator based on quantum dot semiconductor optical amplifiers

Limei Zhang
Zhi Wang
Lanlan Liu



Ultrahigh bit-rate all-optical multibit correlator based on quantum dot semiconductor optical amplifiers

Limei Zhang

Zhi Wang

Lanlan Liu

Beijing Jiaotong University

Institute of Optical Information, School of Science

Beijing 100044, China

E-mail: lmzhang@bjtu.edu.cn

Abstract. An all-optical multibit correlator using the multistage cascaded quantum dots semiconductor optical amplifiers Mach-Zehnder interferometer (QD-SOA MZI) is presented with the example of an 8-bits correlator. The simulations demonstrate the correlator pulse with ultrahigh quality at the bit rate of 500 Gbps. For the ultrahigh bit-rate applications, the ultrafast dynamics of the QD-SOA are investigated with the pulse/spectra distortion, gain dynamics, phase dynamics, and the frequency chirp of the optical pulse. All-optical logical gates XOR and AND based on the QD-SOA MZI are simulated with the consideration of many nonlinear dynamics, such as the carrier injection, carrier depletion, carrier density fluctuation, carrier heating, and the spectra hole-burning in the rate equations scheme. © 2013 Society of Photo-Optical Instrumentation Engineers (SPIE) [DOI: [10.1117/1.OE.52.11.116104](https://doi.org/10.1117/1.OE.52.11.116104)]

Subject terms: all-optical signal processing; all-optical multibit correlator; quantum dot semiconductor optical amplifier.

Paper 131197 received Aug. 8, 2013; revised manuscript received Oct. 11, 2013; accepted for publication Oct. 14, 2013; published online Nov. 6, 2013.

1 Introduction

With the increasing demand for all-optical networking, optical header recognition has become a key approach that enables optical routing in ultrahigh line-speed photonic packet-switched networks.¹ Optical header recognition based on time domain optical correlation has recently attracted great attention. The all-optical logic gates are used widely in the header recognition. Among the logic gates, all-optical XOR is considered to be fundamental as it is a key technology to implement primary systems for address and header recognition. Various configurations of optical logic gates have been reported that utilize the ultrafast nonlinear properties of the semiconductor optical amplifier (SOA), such as the interferometric structures such as the terahertz optical asymmetric demultiplexer² and the ultrafast nonlinear interferometer.³ These schemes have been shown to have some advantages, but they are difficult to control or construct, and polarization states or random phase changes are critical for their output performance.⁴ Among interferometric structures, the SOA-Mach-Zehnder interferometer (MZI) structure using XPM is the most promising candidate due to its attractive features of low-energy requirement, simplicity, compactness by integration capability, and stability. In addition, it has the merits of high extinction ratio (ER), regenerative capability, high-speed operation, and low chirp.⁴ The XOR gate has been demonstrated at 40 Gbps (Ref. 5) using SOA-MZI differential schemes experimentally. But it has strong speed limitations for the SOAs' slow recovery time.

Quantum dots (QD)-SOA are currently attracting attention for the characteristics of high gain, high saturation output power, low noise figure, and fast carrier recovery.⁶⁻⁸ The suppression of pattern effects in QD-SOAs shows promise for high speed applications.^{9,10} Unlike bulk and quantum

well materials, QDs have discrete energy levels; it is the carrier capture and relaxation dynamics between these levels that will constitute the intrinsic limiting device bandwidth.¹¹ High-speed optical amplifier, optical switching, and wavelength conversion are realized based on the high-speed dynamics characteristic of QD-SOA (Refs. 12 and 13). All-optical circuits for packet compression and decompression are proposed for DPSK packets using optical delay lines and QD-SOA MZI structures by Meleiro et al.¹⁴ Ma et al. realize the AND, XOR, and NOT logic using QD-SOA MZI (Ref. 15) with the consideration of a simple three-level system.

When a short pulse passes through SOA, the gain decreases rapidly, and then recovers gradually. For the high-speed operation of LDs and SOAs, a fast gain recovery is essential. The gain recovery for the QD-SOA was extremely fast in contrast to a recovery time for commercially available bulk SOAs (Ref. 16). Park and Kim¹⁶ measured the gain and phase dynamics of a high quality QD-SOA at various wavelengths from the ground state (GS) to the excited state (ES) using the heterodyne pump-probe technique. In the GS, the fast dominant gain recovery time was 0.7 ps. The amplitude and phase dynamics of the QD, quantum dash, and quantum well devices are experimentally studied by Zilkie and Meier.¹⁷ The QD device is found to have the shortest long-lived gain recovery as well as gain and phase changes.

The gain of the pulse in SOA is related to time. Frequency chirp will occur at the output pulse because the phase change is different at different positions of the pulse. Dynamics of gain, phase, and frequency chirp can help to study the physical process of distortion of the pulse, which is also important to the all-optical signal processing and device performance.¹⁸

We will investigate the dynamics of the QD-SOA using the finite differential method (FDM) based on the transitions between energy levels of the conduction band (CB), the valence band (VB), or the wetting layer (WL). The gain

dynamics, phase dynamics, and the frequency chirp of the output pulse are shown in detail. A QD-SOA MZI and some logic gates will be discussed, and an 8-bits all-optical correlator will be demonstrated with some simulations for the photonic integrated cascaded QD-SOA MZIs. A correlative optical pulse will output only when an address matching occurs and can be used as a trigger for the following signal processors in an all-optical packet switching node/router.

2 Physical Model and Algorithm

The energy level structure and physical model are established according to Ref. 19. Our investigated device is an InAs/GaAs QD-SOA. The active region of this QD-SOA consists of seven-stacked layers of self-assembled InAs QDs that are grown on a GaAs substrate. The QD layers have a surface density of $5.0 \times 10^{10} \text{ cm}^{-2}$ and are covered with a 5-nm thick InGaAs capping layer. In this QD-SOA, the self-assembled QDs have three nondegenerate energy levels in the CB and eight nondegenerate energy levels in the VB. The energy separation between the adjacent levels in the CB is 70 meV and between the adjacent levels in the VB is 10 meV. The GS of InAs QDs emits near $1.3 \mu\text{m}$. Besides the states of the QDs, there are two energy levels in the CB and VB corresponding to the WL state.¹⁹

The photon rate equation for the propagating wave is¹⁹

$$\frac{\partial S}{\partial z} = gS - \alpha S, \quad (1)$$

where α is the waveguide loss, $S = S(z, t)$ is the density of propagating photons per unit volume, and $g = g(z, t)$ is the modal gain and is given by

$$g = \sum_{j=0}^H g_j (f_j^n + f_j^p - 1),$$

where $f_j^n = f_j^n(z, t)$ and $f_j^p = f_j^p(z, t)$ are the occupation probabilities for the j 'th state of the electron's and hole's energy states, respectively, H is the number of transitions, and the gain dispersion effect is taken into account where

$$g_j = g_j^{\max} \frac{\hbar\omega_j^{\max}}{\hbar\omega} \exp\left[-\frac{(\hbar\omega - \hbar\omega_j^{\max})^2}{2\sigma_j^2}\right],$$

where g_j^{\max} is the maximum gain coefficient for the j 'th transition, σ_j is the inhomogeneous line broadening, $\hbar\omega$ is the photon energy of the input signal, and $\hbar\omega_j^{\max}$ is the energy corresponding to the gain peak for the j 'th transition.

The rate equation for electrons in the GS of the CB is

$$\frac{\partial f_0^n}{\partial t} = (R_{1,0}^{nc} - R_{0,1}^{ne}) - R_0^{sp} - R_0^{st}. \quad (2)$$

The rate equation for electrons in the i 'th ES is

$$\frac{\partial f_i^n}{\partial t} = (R_{i+1,i}^{nc} - R_{i,i+1}^{ne}) - (R_{i,i-1}^{nc} - R_{i-1,i}^{ne}) - R_i^{sp} - R_i^{st}, \quad (3)$$

where $R_{i+1,i}^{nc} = R_{i+1,i}^{nc}(z, t)$ is the electron capture rate from the $(i+1)$ 'th energy state to the i 'th state and $R_{i,i+1}^{ne} = R_{i,i+1}^{ne}(z, t)$ is the electron escape rate from the i 'th energy

state to the $(i+1)$ 'th energy state. The capture and escape rates for electrons in the i 'th electron state are given by

$$R_{i+1,i}^{nc} = \frac{(1 - f_i^n) f_{i+1}^n}{\tau_{i+1,i}^n} (a_{i+1,i}^n + c_{i+1,i}^{np} \omega_p + c_{i+1,i}^{nn} \omega_n),$$

$$R_{i,i+1}^{ne} = \frac{f_i^n (1 - f_{i+1}^n)}{\tau_{i,i+1}^n} (a_{i,i+1}^n + c_{i,i+1}^{np} \omega_p + c_{i,i+1}^{nn} \omega_n),$$

where $\tau_{i+1,i}^n$ is the electron capture time from the $(i+1)$ 'th energy state to the i 'th state in the CB, $\tau_{i,i+1}^n$ is the electron escape time from the i 'th energy state to the $(i+1)$ 'th state, $\omega_p = \omega_p(z, t)$ and $\omega_n = \omega_n(z, t)$ are the occupation probability of the VB and CB WL states, respectively, $c_{i+1,i}^{np}$ and $c_{i+1,i}^{nn}$ are the electron-hole and the electron-electron Auger-assisted coefficients, respectively. R_i^{sp} and R_i^{st} are the spontaneous and stimulated emission rates, respectively, and are given by

$$R_i^{sp} = \frac{f_i^n f_i^p}{\tau_{iR}} (a_{ii}^n + c_{ii}^p f_i^p + c_{ii}^n f_i^n) \quad R_i^{st} = \frac{v_g g_i}{N_Q} (f_i^p + f_i^n - 1) S,$$

where τ_{iR} is the spontaneous radiative lifetime in the i 'th energy state, a_{ii}^n is the phonon-assisted coefficient, c_{ii}^p is the Auger-assisted coefficients, and N_Q is the density of self-assembled QDs per unit volume.

We assume that electrons are injected directly into the WL and afterward are captured in QD levels. The rate equation for the WL in the CB is

$$\frac{\partial \omega_n}{\partial t} = \frac{I}{q V_a N_{\text{WL}}} - (R_{\omega_n,2}^{nc} - R_{2,\omega_n}^{ne}) - R_{\omega_n}^{sp}, \quad (4)$$

where q is the electron charge, V_a is the volume of the WL, and N_{WL} is the maximum carrier density at the WL.

InAs QDs have eight energy states in the VB. The rate equations for holes in the GS and first two ESs of the VB are similar to Eqs. (2) and (3), except that the superscript n is replaced by p . The rate equation for the k 'th hole state ($k \geq 3$) is given by

$$\frac{\partial f_k^p}{\partial t} = (R_{k+1,k}^{pc} - R_{k,k+1}^{pe}) - (R_{k,k-1}^{pc} - R_{k-1,k}^{pe}), \quad (5)$$

where $R_{k+1,k}^{pc} = R_{k+1,k}^{pc}(z, t)$ is the hole capture rate from the $(k+1)$ 'th state to the k 'th energy state of the VB. Similarly, $R_{k,k+1}^{pe} = R_{k,k+1}^{pe}(z, t)$ is the hole escape rate from the k 'th energy state to the $(k+1)$ 'th energy state.

The rate equation for holes in the WL is given by

$$\frac{\partial \omega_p}{\partial t} = \frac{I}{q V_a N_{\text{WL}}} - (R_{\omega_p,7}^{nc} - R_{7,\omega_p}^{ne}) - R_{\omega_p}^{sp}. \quad (6)$$

In order to get the longitudinal and temporal evolutions of input optical pulses in the active region of a QD-SOA, the FDM is employed to solve the rate equations numerically. In this method, the length of a QD-SOA is divided into M identical sections in the z -direction. In each section, the physical quantities and modal gain are assumed to be constant and, therefore, the photon density at the end of each section is computed based on this assumption. In our simulations,

the algorithm will be implemented with three steps. First, the initial values of the occupation probabilities will be calculated by solving the rate equations of the QD-SOA at a steady-state condition, i.e., for $\partial/\partial t = 0$ and $S_{in}(t) = 0$. Second, the FDM will be employed to solve the rate equations numerically with the initial values to get the occupation probabilities at every level. Third, the photon rate and, hence, the output optical pulse will be obtained with the gain dynamics and the phase dynamics at the end of the last section.

3 Dynamics of the QD-SOA

3.1 Gain Dynamics

A Gaussian pulse with the power $P_{in} = P_0 \exp(-t^2/T_0^2)$, where T_0 is the half-width (25 ps in the simulations), is injected into the QD-SOA, the wavelength of the optical pulse is 1300 nm, and other parameters used in the simulations are shown in Table 1.

Figure 1(a) shows the normalized input pulse and output pulse of the QD-SOA when the peak power of the Gaussian pulse is 0.05 W. As the pulse experiences different gains at different times and different z positions due to the nonuniform distribution of the carrier density and the occupation probabilities along the QD-SOA, the pulse shape becomes asymmetric with a sharper leading edge and a flatter trailing edge. Figures 1(b) and 1(c) show the spectra of both input and output signals with the input peak power of 0.05 and 0.1 W, respectively. It shows that the output spectrum is not a Gaussian one, and is even split asymmetrically because

of the nonlinearities of the QD-SOA, and there will be more peaks when the input power is greater. As the input pulse energy increases, the first peak on the red side ($\Delta\Omega_r$) of the center frequency will shift to the center, and the first peak on the blue side ($\Delta\Omega_b$) will shift against the center, i.e., both peaks will blue shift due to the strong nonlinearities, such as self-phase modulation and four wave mixing. Figure 1(d) shows the relationships between the frequency shift ($\Delta\Omega_r$, $\Delta\Omega_b$) and the input peak power, and the spectrum split and blue shift are both demonstrated in it.

The modal gain of the pulse through a QD-SOA can be calculated by $G = \exp[\int(g - \alpha)dz]$, and Fig. 2(a) shows the gain dynamics of the Gaussian pulses with different input peak powers. Before the coming of the pulse, the gain is the small signal gain (G_0) and it is the greatest. With the coming of the optical pulse, the stimulated emission is enhanced and the photon rate increases, so the carriers will be depleted and the occupation probability on the GS will decrease, which causes the QD-SOA to be saturated almost at the same time as the pulse coming. The larger the peak power is, the deeper the saturation is, and so the difference between the small signal gain and the saturated gain is greater. After the pulse, the carrier and hence the gain recovers gradually, and the recovery is much slower than the pulse leaving. Figure 2(b) shows the dynamic gain of the pulse through QD-SOAs with different lengths of the active area of 3, 4, and 5 mm, and the peak power is exactly the same as 0.1 W. With the active area lengthening, the small signal gain increases greatly, but the saturated gain

Table 1 Parameters in the simulations.

Parameters	Value	Parameters	Value	Parameters	Value
L	3 mm	τ_{0R}	0.2 ns	g_0^{\max}	14 cm ⁻¹
W	2 μ m	τ_{1R}	0.2 ns	g_1^{\max}	20 cm ⁻¹
Lw	0.1 μ m	$\tau_{\omega R}$	0.2 ns	g_2^{\max}	~0 cm ⁻¹
H	2	$\tau_{1,0}^n$	8 ps	ϵ_{CH}	1 \times 10 ⁻¹⁸ cm ³
α	4 cm ⁻¹	$\tau_{2,1}^n$	2 ps	ϵ_{SHB}	1 \times 10 ⁻¹⁸ cm ³
q	1.602 \times 10 ¹⁹ C	$\tau_{3,2}^n$	0.8 ps	α_{SHB}	0
ν_g	8.45 \times 10 ⁹ cm/s	$\tau_{0,1}^n$	80 ps	α_{TPA}	0
σ_j	30 meV	$\tau_{1,2}^n$	20 ps	c_{ii}^p	0.2
N_{WL}	5.4 \times 10 ¹⁷ cm ⁻³	$\tau_{2,3}^n$	8 ps	$c_{1,0}^{nn}$	27
N_Q	2.5 \times 10 ¹⁷ cm ⁻³	$\tau_{k+1,k}^p$	0.5 ps	$c_{1,0}^{np}$	175
$\hbar\omega_0^{\max}$	0.962 eV	$\tau_{k,k+1}^p$	5 ps	$c_{2,1}^{nn}$	7
$\hbar\omega_1^{\max}$	1.042 eV	$a_{j,i}^{np}$	1	$c_{2,1}^{pp}$	35
$\hbar\omega_2^{\max}$	1.122 eV	$a_{i,j}^{np}$	1	α_{CH}	1.2
J	4			α_{LEF}	4

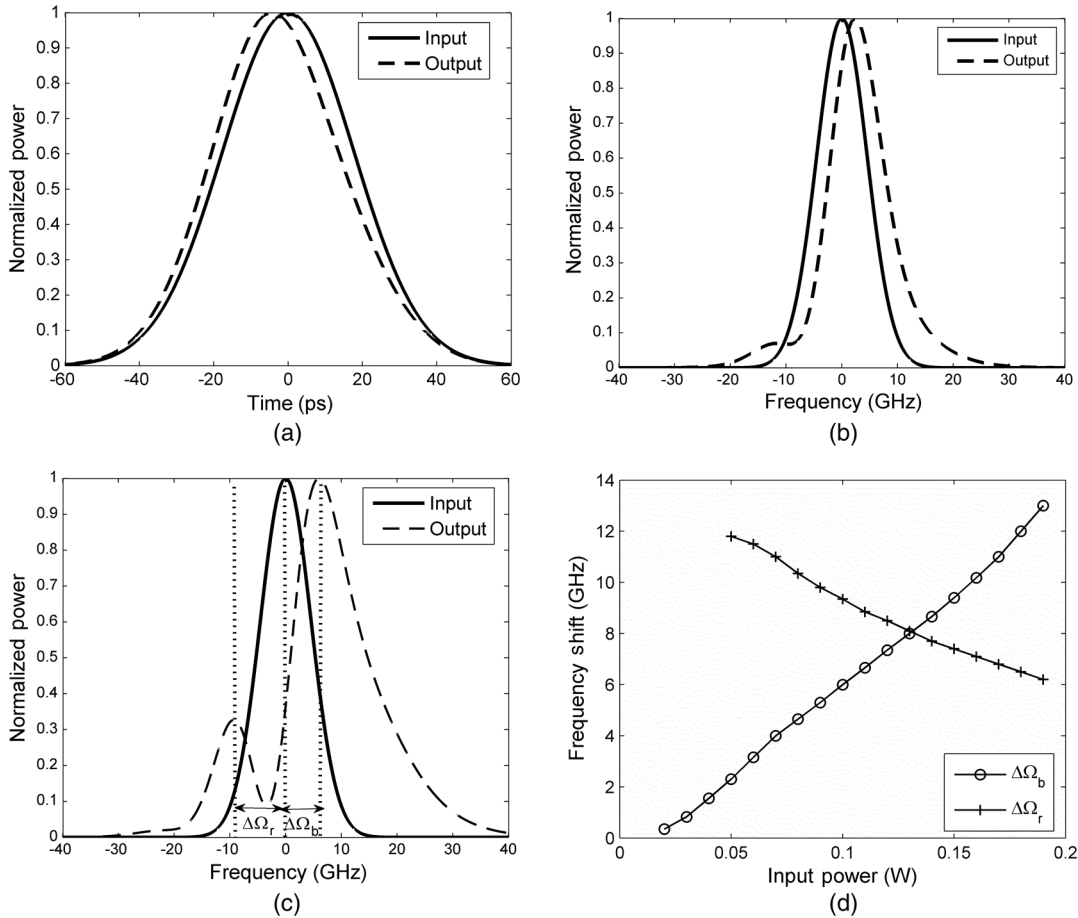


Fig. 1 The pulse (a) and spectra (b and c for peak power of 0.05 and 0.1 W distortion), (d) is the relationship between the frequency shift and the peak power.

(G_{sat}) is almost unchanged, which means the saturation process gets faster with a longer active area.

3.2 Phase Dynamics and Frequency Chirp

The gain of SOA includes the contributions from the carrier density pulsation (CDP) and the nonlinear processes as the

carrier heating (CH), the spectral hole burning (SHB) effects, and two photons absorption (TPA). The suppression of the gain coefficient brought by nonlinear CH and SHB effects can be expressed as $g = g_{CDP} + g_{CH} + g_{SHB} + g_{TPA}$, where g is the total gain, g_{CDP} is due to inter-band processes (e.g., spontaneous emission, stimulated emissions, and absorption) dependent on the carrier density, whereas

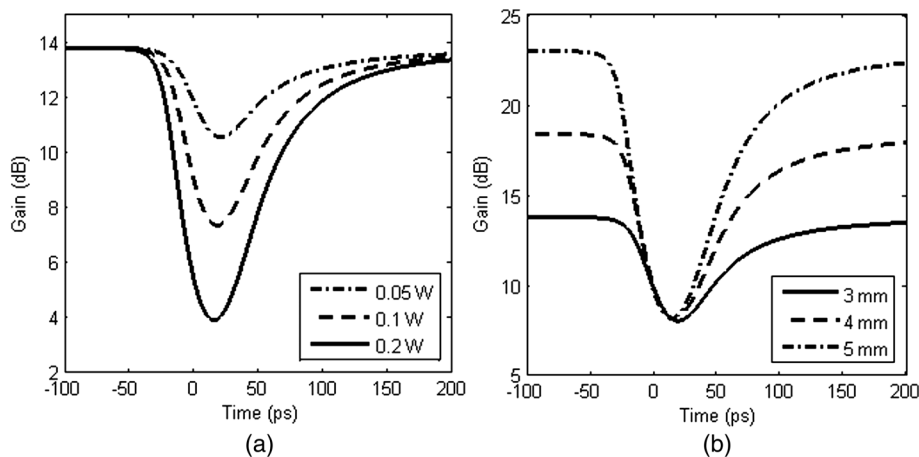


Fig. 2 Gain dynamics for different input peak powers (a) and different SOA lengths (b).

g_{CH} , g_{SHB} , and g_{TPA} are because of the intra-band processes (e.g., CH, SHB, and TPA). g_{CH} , g_{SHB} , and g_{TPA} are proportional to the instantaneous light intensity $S(t)$: $g_{CH} = -\epsilon_{CH}gS(t)$, $g_{SHB} = -\epsilon_{SHB}gS(t)$, $g_{TPA} = -\epsilon_{TPA}gS(t)$, ϵ_{CH} , ϵ_{SHB} , and ϵ_{TPA} are the gain suppression factors for CH, SHB, and TPA effects.

Because of the Kramers–Kronig relationship between the real and imaginary parts of the refractive index of the QD-SOA, the phase change φ of the signal through the QD-SOA is $\varphi = -\int(\alpha_{LEF}g_{CDP} + \alpha_{CH}g_{CH} + \alpha_{SHB}g_{SHB} + \alpha_{TPA}g_{TPA})dz/2$,²⁰ where α_{LEF} is the usual linewidth enhancement factor associated with the inter-band transition, and α_{CH} , α_{SHB} , and α_{TPA} are the linewidth enhancement factors corresponding to the intra-band process as CH, SHB, and TPA. Then, the frequency chirp $\delta\omega$ of the optical signal can be obtained by $\delta\omega = -d\varphi/dt$ due to the phase dynamics.

Figure 3(a) shows the phase dynamics of the Gaussian pulses with different peak powers amplified by the QD-SOA. It is obvious that the higher the peak power is, the

greater the dynamics range of the phase is. Figure 3(b) shows the temporal dynamics of gain and phase of the Gaussian pulse with the peak power of 0.1 W. The phase dynamics is a complicated curve which can be divided into two prominent components (fast and slow) with different change directions. Figure 3(b) shows that there is an advanced time between the fast part of the phase dynamics and the gain dynamics, and a delay between the slow part of the phase dynamics and the gain dynamics. In fact, the phase preceding response part is dominated by the fast effects of the SHB and TPA and the succeeding slow part is determined by the CH.

The time difference t_1 and t_2 , as shown in Fig. 3(b), are defined as the advanced time and the delay, and their dependences on the input peak power and the SOA length are shown in Figs. 3(c) and 3(d). It demonstrates that the advanced time t_1 increases with the input power and the SOA length, while the delay time t_2 decreases with the input power and the SOA length. The phenomena of the out-of-synchronism between

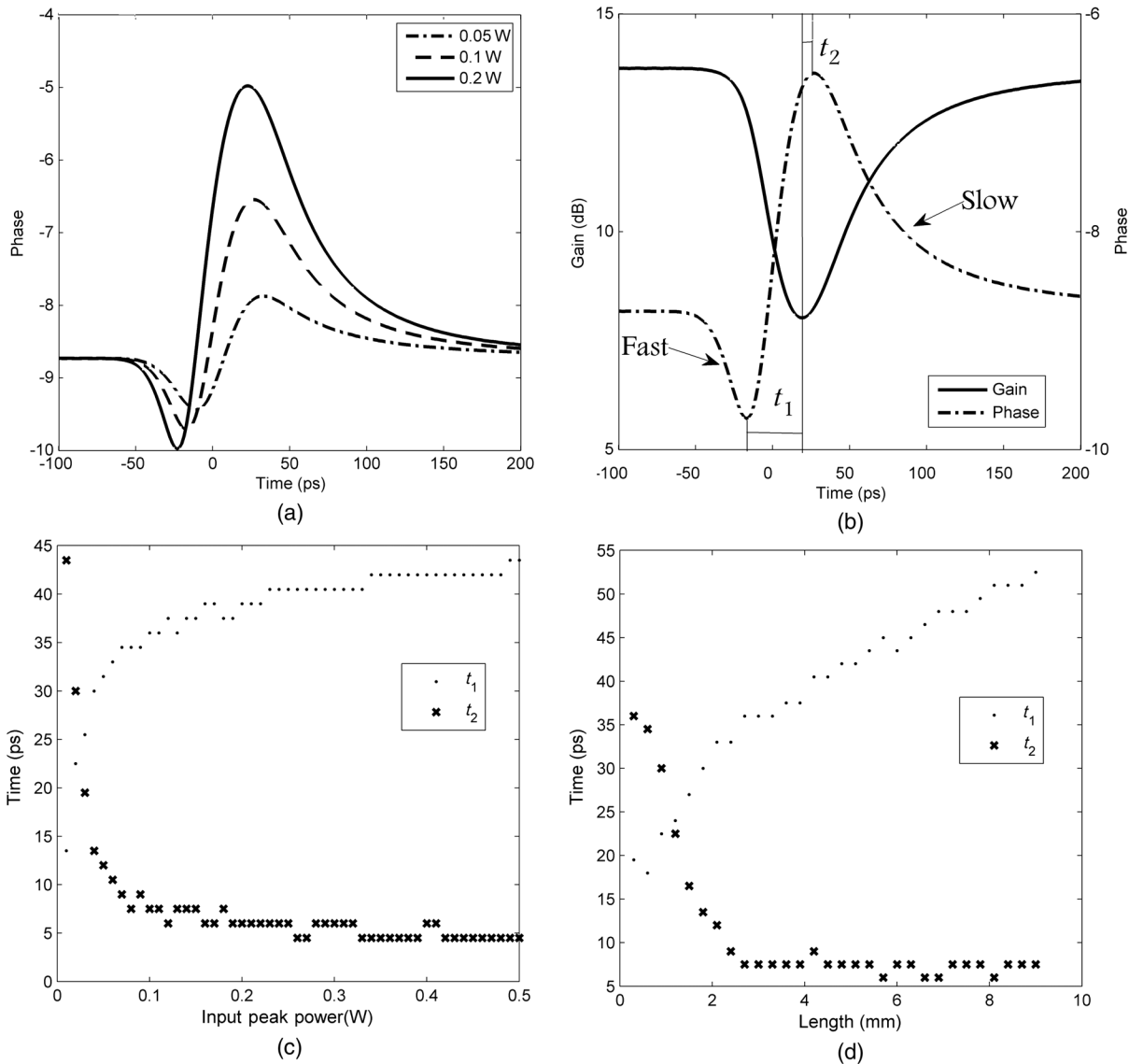


Fig. 3 Phase dynamics for different input peak powers (a), out-of-synchronism between the temporal dynamics of gain and phase (b), the dependence of the advanced (t_1) and delay (t_2) time on the input peak power (c) and the SOA length (d).

the phase and gain will result in some new ideas for ultrahigh-speed optical signal processing, especially for the novel modulation format signals, such as QPSK or DP-QPSK, and for the future ultralong haul optical transmission systems.

The normalized frequency chirp $\delta\omega T_0$ is shown in Fig. 4(a) for the input peak power is 0.05, 0.1, and 0.2 W (QD-SOA is 3-mm long), and in Fig. 4(b) for the SOA length is 3, 4, and 5 mm (the peak power is 0.1 W). It shows the blue shift of the leading edge, the red shift of the middle part, and the blue shift of the trailing edge. The chirp increases with the input power and the SOA length.

From Figs. 2 and 3, when the input pulse peak power is greater, or the SOA is longer, the gain saturation dynamics are deeper and faster. The faster the phase and gain dynamics are, the greater the chirp is. So the chirp increases with the input peak power and the SOA length. In order to show the dependence of the frequency chirp, the dependence of both the maximum positive and negative frequency chirp of the Gaussian pulse on the input peak power and the SOA length are shown in Figs. 5(a) and 5(b). During the

simulations, the current density in the QD-SOA keeps constant for different lengths.

4 All-Optical Logic Using QD-SOA MZI

Based on the ultrafast gain and phase dynamics of the QD-SOAs, an MZI is usually adopted to implement ultrahigh speed all-optical signal processing. A QD-SOA MZI is composed of two arms with a QD-SOA on each, shown as Fig. 6, two series of optical signals A and B at different wavelengths (λ_1, λ_3) are coupled into the upper arm and the lower arm, respectively, and the probe beam at λ_2 is equally split and coupled into both QD-SOAs. The probe beams experience nonlinear gain modulation or phase modulation due to the nonlinear interaction with signal A and B in both QD-SOAs on both arms, both beams will interfere at the output coupler of the MZI, so it will be an XOR logic gate with a band pass filter (BPF) at λ_2 following the MZI.

The BPF screens out the light at wavelength λ_1 and λ_3 , and the output at λ_2 can be expressed as

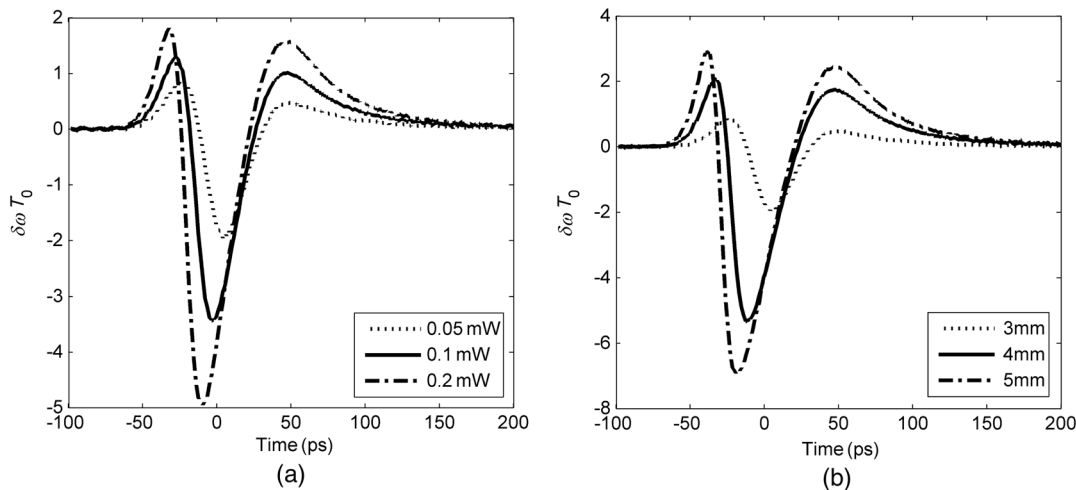


Fig. 4 Frequency chirps of the Gaussian pulse for different input peak powers (a) and different SOA lengths (b).

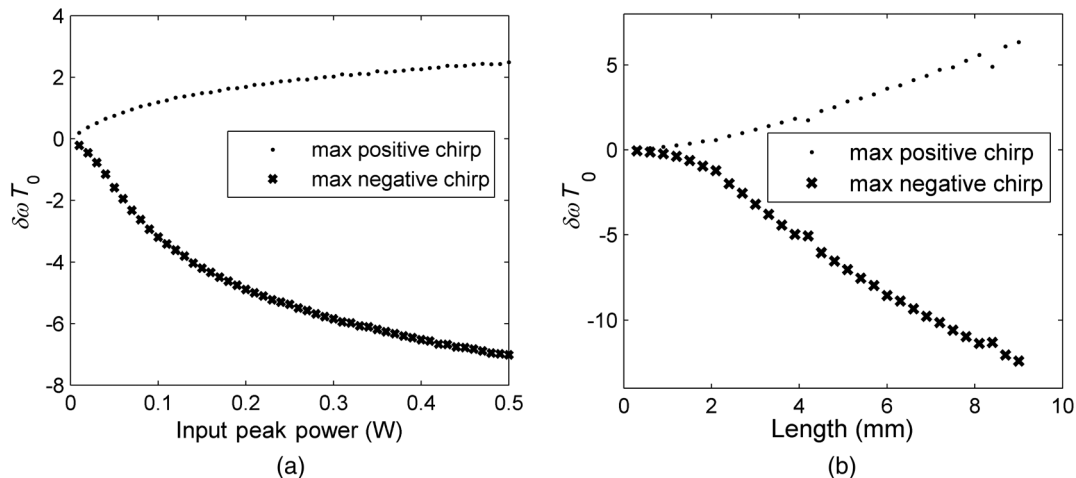


Fig. 5 Dependence of the maximum frequency chirp on the input peak power (a) and SOA length (b).

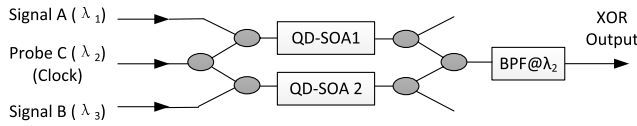


Fig. 6 Scheme of XOR logic.

Table 2 True value of XOR and NOT with the QD-SOA MZI.

A	B	A XOR B	NOT A
0	0	0	
0	1	1	1
1	0	1	
1	1	0	0

$$P_{out}(t) = \frac{P_{probe}(t)}{4} \left\{ G_1(t) + G_2(t) - 2\sqrt{G_1(t)G_2(t)} \cos[\phi_1(t) - \phi_2(t)] \right\}, \quad (7)$$

where $P_{probe}(t)$ is the time-dependent power of the probe beam. G_1 , G_2 , ϕ_1 , and ϕ_2 are the gain and phase changes

of the probe beam on both the arms. We put data streams A and B into ports 1 and 2, respectively and a much weaker clock as probe (control) beam. When $A = B$, then $G_1 = G_2$, $\phi_1 = \phi_2$, $P_{out} = 0$; if $A \neq B$, $P_{out}(t) \neq 0$, its temporal shape is similar to the input control beam pulse as a result of fast gain response. Then, the QD-SOA MZI is an XOR gate. Similar to XOR, the logic NOT operation can be realized by the same MZI scheme if a clock input is used as data B.¹⁵ The true value of both XOR and NOT is shown in Table 2.

4.1 Logic XOR

In order to check the logic XOR, two data series (A and B) with the Gaussian shape of 500 Gbps are supposed to input to the QD-SOA MZI, with the pulse width 0.8 ps and the pulse energy 0.05 pJ. The signal-to-noise ratio and the ER of the input signal are both set to be 20 dB, the pulse energy of the probe (clock) is 0.002 pJ, and the pulse width is also 0.8 ps. Other parameters for the simulations are shown in Table 1.

Figure 7(a) shows the gains and phases of signal A and signal B. Because of the effect of recovery time of the electron and the hole, the gain reduces gradually, and cannot recovery to its small signal gain. The sequence of the logic XOR (inputs A and B, output XOR) is shown in Fig. 7(b), and the eye-diagram of the output is shown in Fig. 7(c). Even the gain dynamics for both signals A and B are gently time dependent due to the limited-carrier lifetime, so the phase dynamics show much less dependence, and the optical logic XOR has a high quality factor (Q -factor) of

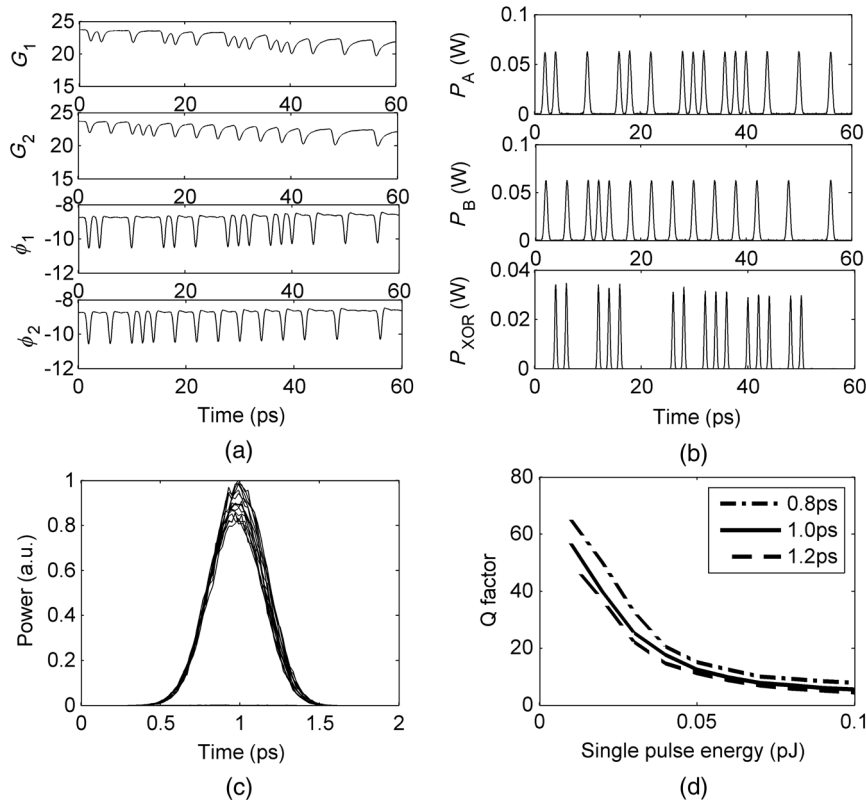


Fig. 7 Gain and phase dynamics of the signal A and signal B (a), sequence diagram of the XOR logic (b), and the eye-diagram of the output (c), (d) is the dependence of the Q -factor on the pulse width and the single pulse energy.

about 15 in our simulations. The output Q -factor depends on the width and energy of the input pulse, and it decreases with the width and the single pulse energy, as shown in Fig. 7(d). Of course, the output Q -factor also depends on the input Q -factor, which will be discussed in our future works.

4.2 Logic NOT

The simulation conditions of the logic NOT are similar to the XOR gate, but the data B is changed to 500 Gbps Gaussian pulse clock series. The pulse width of data A, B, and the probe are all 0.5 ps, the single pulse energy of both A and B is 0.02 pJ, and the single pulse energy of the probe is 0.002 pJ. Figures 8(a) and 8(b) are the output sequence of the logic NOT and the eye-diagram, from which the Q -factor is calculated to be about 10.44.

5 Multibit All-Optical Correlator

By employing the QD-SOA MZI structure, as shown in Fig. 6, a multibit all-optical correlator can be implemented with a cascaded multistage logic gates. The proposed structure of a 8-bits all-optical correlator, shown as Fig. 9, is composed by 9-stage QD-SOA MZIs, where the first one (0-stage) is for logic “NOT(A),” the others (1 stage to 8 stage) are for logic XOR. The operation of the correlator could be explained briefly as below.

Eight-bits signal “A,” clock 1, and clock 2 are coupled into the 0-stage QD-SOA MZI to obtain the logic “NOT (A).” “NOT(A)” and 8-bits signal “B” are split into eight channels and input into the following stages of the MZIs. For the 1-stage, “NOT(A)” and signal “B” are synchronized with the control pulse before input into the QD-SOA MZI, and the output signal (Output 1) is the logic XOR between the first bits of both data sequences “NOT(A)” and “B.” The signal “Output 1,” after the power gain or attenuation and the time-delay control, is synchronized with the second bits of both “NOT(A)” and “B” as the control pulse for the 2-stage QD-SOA MZI. Also, the output signal of the n 'th-stage XOR is launched into the $(n + 1)$ 'th-stage XOR as the control pulse synchronized with the $(n + 1)$ 'th bit of the data sequence, then the output of the last stage QD-SOA MZI (the last XOR) is the output of the multibit correlator. The correlator can be expressed as

$$\text{Output} = \begin{cases} 0, & \text{if } A \neq B \\ 1, & \text{if } A = B \end{cases} \quad (8)$$

Some simulations of the sequence diagrams of the 8-bits all-optical correlator are shown in Fig. 10 for a few different

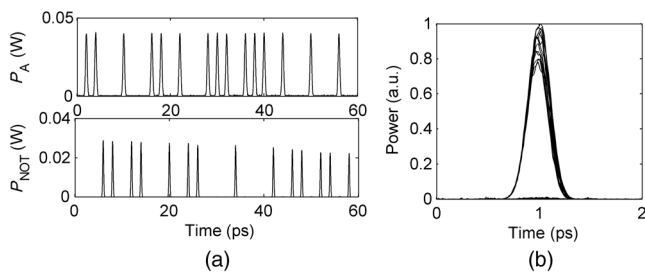


Fig. 8 Sequence diagram of the logic NOT (a) and the eye-diagram of the output (b).

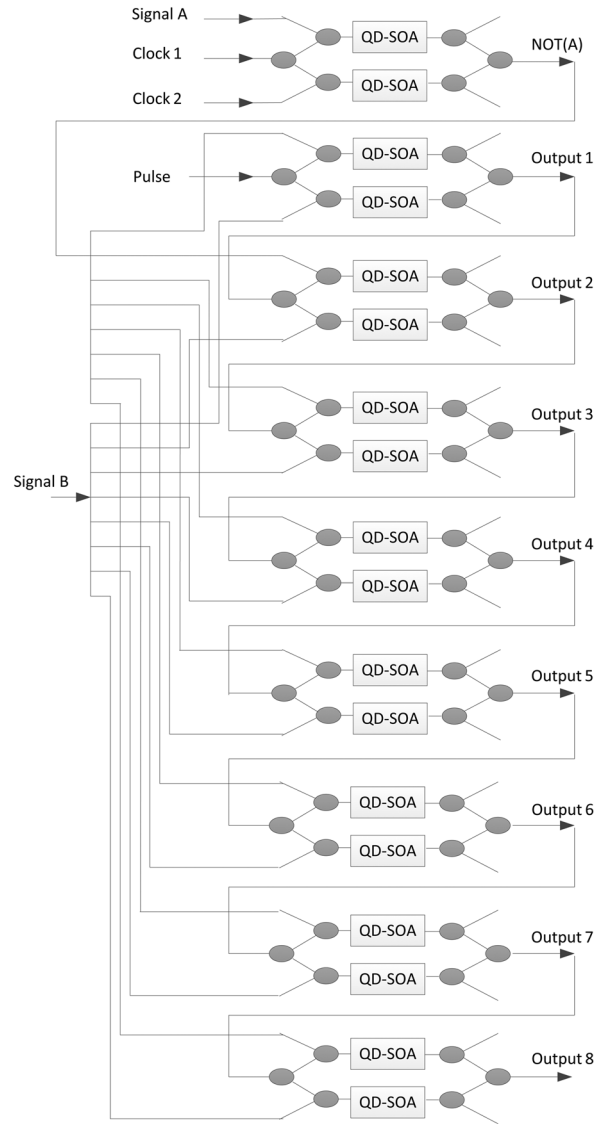


Fig. 9 Scheme of 8-bits correlator with the multistage cascaded QD-SOA MZIs.

series of signal A and B, which are 8-bits RZ format intensity-modulated at 500 Gbps. The pulse energy of signal A, signal B, and clock 2 are 0.05 pJ, and the pulse energy of clock 1 and the control pulse are 0.002 pJ. The $1/e$ pulse widths of all the signals are 0.5 ps.

The output of the 0-stage QD-SOA MZI is “NOT(A),” which is an 8-bits RZ sequence. The input $A = 10110011$, $B = 10111010$ (from left to right), and the correlator output “Null” are illustrated in Fig. 10(a). In order to clearly show the logic details in the 8-stages correlator, Figs. 10(b) and 10(c) give us the output sequence at every XOR stage. The output from the stage 1 to stage 4 is “Mark” (about 17 dB m) because the first 4 bits are same, and the other stages output “Null” (<0 dB m at stage 5, -4 dB m at stages 6 and 7, -40 dB m at stage 8) because the fifth bits for A and B are different.

Figures 10(d), 10(e), and 10(f) show the correlator outputs for three different sequences as $A = B = 10100010$, $A = B = 11111111$, and $A = \bar{B} = 10010010$. It can be seen

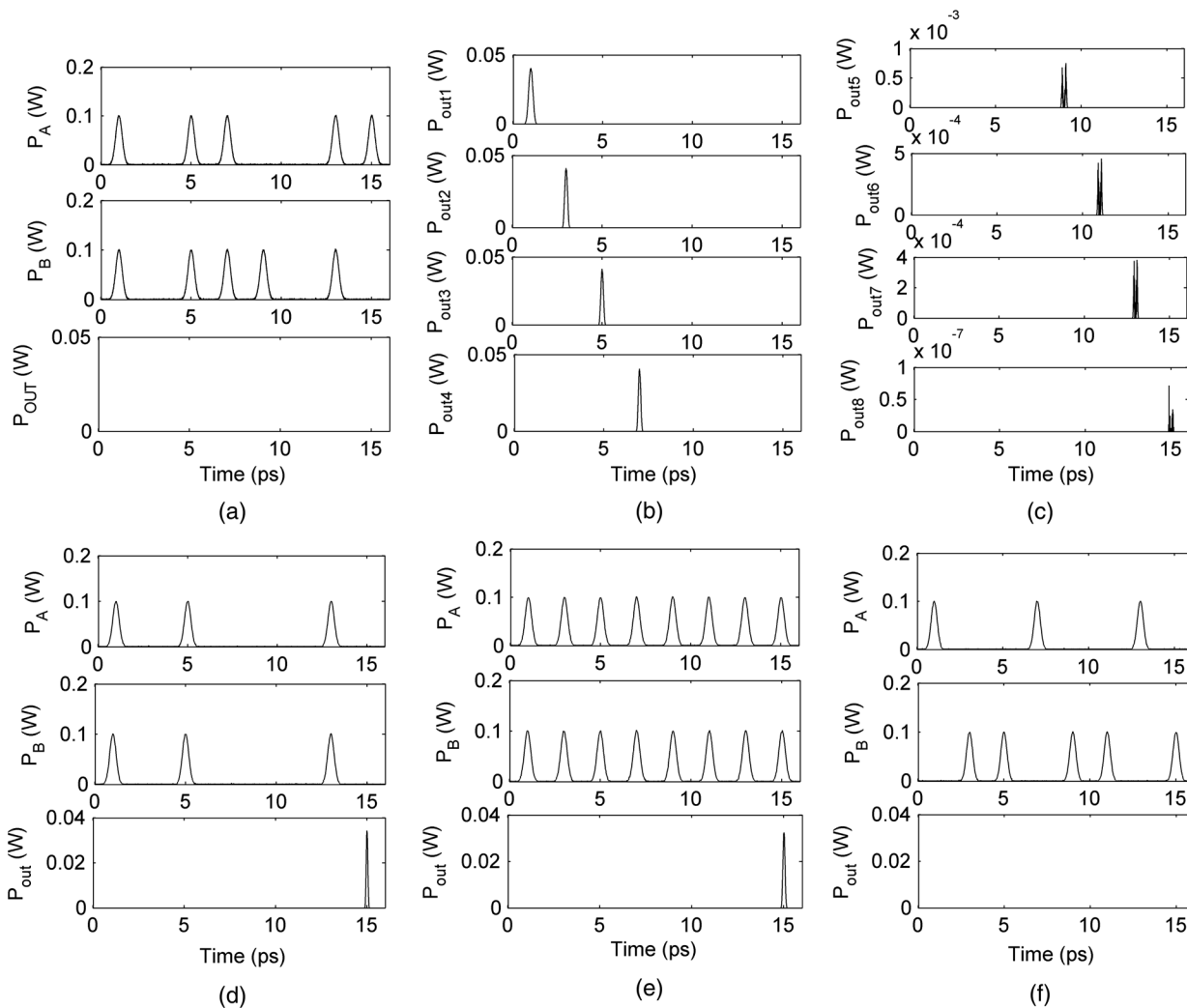


Fig. 10 Sequence diagram of the 8-bit all optical correlator. (a) $A = 10110011$, $B = 10111010$, output "Null"; (b) output at stage 1 to 4; (c) output at stage 5 to 8; (d) $A = B = 10100010$; (e) $A = B = 11111111$; (f) $A = B = 10010010$.

that only one optical pulse at the 8th time-slot outputs from the correlator when $A = B$, and the correlator pulse has much higher ER with about 0.1-ps width.

6 Conclusion

The ultrafast dynamics of the QDs-SOAs are numerically simulated with the pulse/spectra distortion, gain dynamics, phase dynamics, and the frequency chirp of the optical pulse. The spectrum will split and blue shift more with greater input peak power. The dynamics (both saturation and recovery) of the phase are faster than that of the gain, but the over-shooting during the phase recovery leads to a slowly steady progress, and the advanced time difference between the phase and gain dynamics increases with the input peak power and the SOA length. There are red shifts in the middle part of the pulse and blue shifts at both leading and tailing parts, and the frequency chirp becomes greater with the input peak power and the SOA length. The ultra fast dynamics of the QD-SOA comes from the strong non-linearity and will lead to some new ideas for ultrahigh speed all-optical signal processing and some novel devices.

An all-optical logical XOR gate based on MZI using QD-SOAs is established and simulated. Nonlinear dynamics including CH and spectra hole burning are taken into account together with the carrier injection, carrier density fluctuation, and carrier depletion in the rate equations scheme. An 8-bits correlator is established using the multistage cascaded QD-SOA MZIs, and the simulations demonstrate the correlator pulse with the ultrahigh quality at the bit rate of 500 Gbps. Of course, based on the similar structure, an N -bits correlator can be implemented with N -stages cascaded QD-SOA MZIs. It is a challenge to fabricate the QD-SOA-MZI and the cascaded structures, but it is believed that it will be realized based on the fabrication process for photonic integrations.²¹

Acknowledgments

This project was supported by the National Natural Science Foundation of China (Grant No. 61077048), Beijing Natural Science Foundation (Grant No. 4132035), Specialized Research Fund for the Doctoral Program of Higher Education (Grant No. 20120009110032), and by the Fundamental Research Funds for the Central Universities (Grant No. 2012JBM103).

References

1. J. E. McGeehan et al., "Multiwavelength-channel header recognition for reconfigurable WDM networks using optical correlators based on sampled fiber Bragg gratings," *IEEE Photonics Technol. Lett.* **15**(10), 1464–1466 (2003).
2. H. J. S. Dorren, G. D. Khoe, and D. Lenstra, "All-optical switching of an ultrashort pulse using a semiconductor optical amplifier in a Sagnac-interferometric arrangement," *Opt. Commun.* **205**(4), 247–252 (2002).
3. C. Schubert et al., "160-Gb/s all-optical demultiplexing using a gain transparent ultrafast-nonlinear interferometer (GT-UNI)," *IEEE Photonics Technol. Lett.* **13**(5), 475–477 (2001).
4. J. Kim et al., "All-optical multiple logic gates with XOR, NOR, OR, and NAND functions using parallel SOA-MZI structures: theory and experiment," *IEEE J. Lightwave Technol.* **24**(9), 3392–3399 (2006).
5. R. P. Webb et al., "40 Gbit/s all-optical XOR gate based on hybrid-integrated Mach-Zehnder interferometer," *Electron. Lett.* **39**(1), 79–81 (2003).
6. O. Qasaimeh, "Optical gain and saturation characteristics of quantum-dot semiconductor optical amplifiers," *IEEE J. Quantum Electron.* **39**(6), 793–798 (2003).
7. D. Klotzkin and P. Bhattacharya, "Temperature dependence of dynamic and DC characteristics of quantum well and quantum dot lasers: a comparative study," *IEEE J. Lightwave Technol.* **17**(9), 1634–1642 (1999).
8. T. W. Berg and J. Mørk, "Quantum dot amplifiers with high output power and low noise," *Appl. Phys. Lett.* **82**(18), 3083–3085 (2003).
9. T. Akiyama, N. Hatori, and Y. Nakata, "Pattern-effect-free semiconductor optical amplifier achieved using quantum dots," *Electron. Lett.* **38**(19), 1139–1140 (2002).
10. A. V. Uskov, E. P. O'Reilly, and R. J. Manning, "On ultrafast optical switching based on quantum-dot semiconductor optical amplifier in nonlinear interferometers," *IEEE Photon. Technol. Lett.* **16**(5), 1265–1267 (2004).
11. T. Piwonski and I. O'Driscoll, "Gain and phase dynamics of InAs/GaAs quantum dot semiconductor optical amplifier," in *ICTON 2008: 10th Anniversary Int. Conf. Transparent Optical Networks*, Athens, Greece, pp. 145–148 (2008).
12. S. Sygletos and R. Bonk, "Filter assisted wavelength conversion with quantum-dot SOAs," *J. Lightwave Technol.* **28**(6), 882–897 (2010).
13. G. Contestabile and A. Maruta, "Regenerative amplification by using self-phase modulation in a quantum-dot SOA," *IEEE Photon. Technol. Lett.* **22**(7), 492–494 (2010).
14. R. Meleiro et al., "All-optical RZ-DPSK packet compressor and decompressor based on MZI-quantum-Dot-SOA," in *ICTON 2008: 10th Anniversary Int. Conf. Transparent Optical Networks*, Athens, Greece, pp. 71–74 (2008).
15. S. Ma et al., "High speed all optical logic gates based on quantum dot semiconductor optical amplifiers," *Opt. Express* **18**(7), 6417–6422 (2010).
16. J. Park and N. J. Kim, "Gain dynamics of an InAs/InGaAsP quantum dot semiconductor optical amplifier operating at 1.5 μm ," *Appl. Phys. Lett.* **98**(1), 011107 (2011).
17. A. J. Zilkie and J. Meier, "Carrier dynamics of quantum-dot, quantum-dash, and quantum-well semiconductor optical amplifiers operating at 1.55 μm ," *IEEE J. Quantum Electron.* **43**(11), 982–991 (2007).
18. F. Romstad, P. Borri, and W. Langbein, "Measurement of pulse amplitude and phase distortion in a semiconductor optical amplifier: from pulse compression to breakup," *IEEE Photon. Technol. Lett.* **12**(12), 1674–1676 (2000).
19. H. Taleb, K. Abedi, and S. Golmohammadi, "Operation of quantum-dot semiconductor optical amplifiers under nonuniform current injection," *Appl. Opt.* **50**(5), 608–617 (2011).
20. S. Ma et al., "High speed all-optical PRBS generation based on quantum-dot semiconductor optical amplifiers," *Opt. Express* **17**(21), 18469–18477 (2009).
21. A. Rostami, H. Baghban, and R. Maram, *Nanostructure Semiconductor Optical Amplifiers*, Springer-Verlag, Berlin, Heidelberg (2011).



Limei Zhang received her master's degree from Beijing Normal University in 2001. She is a PhD candidate and a lecturer in the School of Science, Beijing Jiaotong University, China. Her interests include physics, optical communications, all-optical signal processing, and semiconductor optical amplifiers.



Zhi Wang received the BSc degree in physics from Beijing Normal University, Beijing, China, in 1993 and the MEng and PhD degrees from Beijing Jiaotong University in 1996 and 2000, respectively. From July 2004 to August 2005, he served as a research associate with the Department of Electronics, The Hong Kong Polytechnic University. From October 2009 to June 2011, he served as a visiting professor with the Department of Electronics and Computer Engineering, the University of California at Santa Barbara. He is currently with the Institute of Optical Information, School of Science, Beijing Jiaotong University, where he is researching in the microstructured optical fibers, optical fiber sensing, all-optical network, all-optical signal processing, and silicon photonics. He is a member of OSA and SPIE.



Lanlan Liu is an associate professor in the Key Laboratory of Luminescence and Optical Information of Ministry of Education, and the Institute of Optical Information, School of Science, Beijing Jiaotong University. She received the BSc degree from the Harbin Normal University in 1992 and MSc degree from the Harbin Institute of Technology in 1995. She had been an advanced visitor researcher from September 2004 to September 2005 in Belarusian State University, Minsk. Her interest includes optical communications, all-optical network, and optical signal processing.